Validation of Human Whole Blood Oximetry, Using a Hyperspectral Fundus Camera with a Model Eye

David J. Mordant,[1] Ied Al-Abboud,[2] Gonzalo Muyo,[2] Alistair Gorman,[2] Ahmed Sallam,[1] Paul Rodmell,[3] John Crowe,[3] Steve Morgan,[3] Peter Ritchie,[4] Andrew R. Harvey,[2] and Andrew I. McNaught[1,5]

PURPOSE. To assess the accuracy of human blood oximetry measurements in a model eye with a hyperspectral fundus camera.

METHODS. Seven human whole blood samples (two arterial, five venous) were obtained, the oxygen saturations measured with a CO oximeter, and the samples inserted into quartz tubes with internal diameters of 100 and 150 μm. The tubes ($n = 20$; ten 100 μm and ten 150 μm) were placed within a model eye in front of a background reflectance surface with reflectivities of 20%, 60%, and 99%. Spectral images at wavelengths between 500 and 650 nm were acquired with a hyperspectral fundus camera and analyzed with an oximetric model to calculate the oxygen saturation of blood within the tubes. The calculated oxygen saturations were compared with the measured oxygen saturations. The effects of the background reflectivity and tube size on the accuracy of the calculated oxygen saturations were evaluated.

RESULTS. Background reflectivity and tube size had no significant effect on the mean oxygen saturation difference ($P = 0.18$ and $P = 0.99$, respectively; repeated-measures, two-way ANOVA). The mean differences (SD) between the measured and calculated oxygen saturations in segments of the 100 and 150 μm tubes overlying the 20%, 60%, and 99% background reflectivities were (100 μm) -4.0% (13.4%), -6.4% (9.9%), and -5.5% (10.2%) and (150 μm) -5.3% (10.8%), -5.2% (10.7%), and -5.2% (10.9%), respectively.

CONCLUSIONS. There was reasonable agreement between the measured oxygen saturation values and those calculated by the oximetry model. The oximetry model could be used to determine the functional health of the retina. (*Invest Ophthalmol Vis Sci.* 2011;52:2851–2859) DOI:10.1167/iovs.10-6217

Hyperspectral imaging combines the spectroscopy and imaging disciplines and enables the acquisition of spectral information from every pixel in the image plane. By measurement of reflectance or absorption spectra, hyperspectral imaging enables chemical identification and quantification by means of the spectral signature.

The retina is considered to be one of the most metabolically active tissues in the human body,[1] and an imbalance between oxygen supply and demand as a result of ischemia is thought to have a role in the pathogenesis of several retinal diseases. Diabetic retinopathy,[2] glaucoma,[3,4] and age-related macular degeneration[5,6] constitute posterior segment diseases that can cause profound visual disability and blindness. Although several studies indicate an ischemic component that may play a major role in the development of sight-threatening lesions within the retina and optic disc,[7-12] such mechanisms are yet to be fully understood.

Numerous attempts have been made to develop a method of measuring the oxygen tension in the retinal vasculature and tissues. These include the use of oxygen-sensitive microelectrodes,[13] phosphorescence quenching,[14-16] and functional magnetic resonance imaging (fMRI).[17] These methods are invasive and have mostly been limited to animal studies. Consequently, direct evidence of hypoxia in the pathogenesis of retinal diseases in humans is limited.

Noninvasive techniques for measuring oxygen in the retinal vasculature have largely evolved from imaging spectrophotometric methods. These techniques exploit the differential spectral absorption characteristics of the two main hemoglobin derivatives, oxy- and deoxyhemoglobin, and are well established in pulse oximetry and CO oximetry.

Since the first reported retinal vessel oximetry experiments conducted by Hickham et al.[18,19] in the late 1950s and early 1960s, various approaches have been undertaken to noninvasively measure the oxygen saturation of blood in the retinal vessels. The methods used have evolved with the availability of newer technologies from standard photography,[18,19] to digital photography,[20-27] to the use of imaging spectroscopy,[28-34] multispectral confocal scanning laser ophthalmoscopes[35-40] and optical coherence tomography.[41] Numerous dual- and multiple-wavelength combinations that are sensitive to changes in oxygen saturation have been used in various imaging systems; however, one of the main challenges of retinal vessel oximetry is the development of a robust and accurate oximetry technique that accounts for the complex interaction of light with the retinal vessels, retinal tissues, and ocular media. As a result,

there is currently no consensus on a method of calculating oxygen saturation in the retinal blood vessels. The importance of in vitro validation experiments in any new retinal oximeter is therefore paramount. In vitro validation of various retinal oximetry systems have been reported with various model eye configurations.[22,26,27,29,37,42–44]

In this study, we used a hyperspectral fundus camera to validate the accuracy of oxygen saturation calculations for arterial and venous human blood of known oxygen saturation in a model eye. We also sought to establish the effects of the background reflectance and blood column thickness on the accuracy of the oxygen saturation calculations.

METHODS

This study was approved by the Gloucestershire Research Ethics Committee (COREC reference, 06/Q2005/131) and all procedures were performed in accordance with the tenets of the Declaration of Helsinki.

The Hyperspectral Fundus Camera

The hyperspectral fundus camera is a commercial fundus camera (CF-60Z; Canon, Tokyo, Japan) in which a liquid crystal tunable filter (VariSpec; CRI, Woburn, MA), located in the optical path of the camera's light source, enables the electronic selection of a combination of desired light wavelengths between 400 and 700 nm. The liquid crystal tunable filter has a bandwidth of 7 nm (full width at half maximum) and is able to change from one wavelength to another in 50 ms. The wavelength selection is controlled with a customized software interface (LabView VI; LabView, National Instruments, Austin, TX) installed on a personal computer. A low-noise, cooled, CCD camera (ORCA-ER; Hamamatsu Photonics KK, Hamamatsu City, Japan), attached to the imaging port of the fundus camera, is used to record a sequence of spectral images between 500 and 650 nm in 2 nm increments.

The Model Eye

A model eye was constructed to simulate the salient optical properties of the human eye (Fig. 1). It is composed of a water-tight black aluminum outer casing and a +62.5 D doublet convex achromatic lens (Thorlabs, Ltd., Cambridgeshire, UK; AC080-016-A1 series) inserted through an opening in its front surface, such that when distilled water is instilled into the model eye chamber to simulate the vitreous, the effective focal length is approximately 22 mm. To determine the effects of the reflectivity on the accuracy of the oxygen saturation calculation, a background surface was built with reflectance (Spectralon; Labsphere Inc., North Sutton, NH) segments with Lambertian albedos of 20%, 60%, and 99%.

Blood-filled, fused quartz tubes (VitroCom, Mountain Lakes, NJ) could be positioned vertically within the model eye, approximately 300 μm in front of the surface of the reflectance background surface. The refractive index of the quartz tube was 1.46. Data were recorded for quartz tubes with internal diameters of 50, 100, and 150 μm (outer diameters of 80, 170, and 250 μm, respectively), which enabled evaluation of the influence of simulated vessel diameter on the accuracy of the oxygen saturation calculations.

The Model Eye Experiments

The model eye was located in the conventional imaging position in front of the hyperspectral fundus camera. A straight metal wire (~100 μm in diameter) placed in front of the reflectance surface was used to help achieve optimal focus. The position of the fundus camera was also adjusted to attain optimal diffuse illumination (i.e., with minimal vignetting) within the model eye.

Two arterial and five venous blood samples, contained in a syringe lined with 2 mL of lithium heparin (LH, 2 mL; Monovette blood collection system; Sarstedt, Beaumont Leys, UK), were col-

lected from seven subjects in the intensive care unit in Cheltenham General Hospital. Blood gas analysis of each sample was performed with a CO oximeter (Gem Premier 4000; Instrumentation Laboratory, Bedford, MA) at the time of collection. A small sample of the blood was inserted into 100 and 150 μm quartz tubes, the ends of the tubes were sealed with petroleum jelly, and the tubes were located in the model eye in front of the reflectance background. Timed-sequence, hyperspectral images were acquired at wavelengths from 500 to 650 nm at 2 nm intervals. This process was repeated with the same blood sample inserted into 50 μm quartz tubes. The duration of each imaging process was on average no more than 5 minutes. Several repeated attempts to fill 50 μm quartz tubes with blood yielded only broken blood columns in the tube, which were considered unsuitable for oximetry, and consequently these images were not included in the study.

To enable the analysis of blood at intermediate oxygen saturation between the higher and lower saturations commonly found in unmixed arterial or unmixed venous blood respectively, three of the venous blood samples were mixed with various volumes of atmospheric air over a period of 30 to 45 minutes. This process resulted in an increase in the measured oxygen saturation of the venous blood samples. Subsequent to the blood gas analysis with the CO oximeter, the small air bubbles were removed from the syringe, which was then sealed to maintain a stable level of oxygenation before its use in the model eye. Samples of this blood were then imaged within the quartz tubes in the model eye, as just described.

Blood gas analyses of all the blood samples were performed again with the CO oximeter after imaging, and the mean spectrophotometric measurement of oxygen saturation before and after imaging was calculated to determine the gold-standard measured oxygen saturation. The mean difference ($\pm$SD) between the measured oxygen saturation before and after imaging was 0.49% ($\pm$0.76%).

In total, 20 blood-filled quartz tubes (ten 100 μm and ten 150 μm) were imaged. Table 1 summarizes the number of blood samples that were imaged for each type of blood and tube size. The measured oxygen saturation range (mean $\pm$ SD) of the arterial and venous blood samples were 97.9% to 98.9% (98.4% $\pm$ 0.7%) and 23.4% to 97.5% (69.7% $\pm$ 25.3%), respectively. The total hemoglobin concentration ranges (mean $\pm$ SD) were 9.9 to 10.7 g/dL (10.3 $\pm$ 0.5) and 7.1 to 18.3 g/dL (13.7 $\pm$ 3.7) for the arterial and venous blood samples, respectively. The hematocrit range (mean $\pm$ SD) of the arterial and venous blood samples were 28.5% to 30.5% (29.5% $\pm$ 1.4%) and 32.5% to 57.5% (46.9% $\pm$ 8.1%), respectively.

Image Processing and Quantitative Oximetry Calculation

All raw spectral images of the model eye were saved in 12-bit portable network graphics (PNG) format. Further processing and analysis of the raw images was performed with commercial software (Mathematica, ver. 5.2; Wolfram Research, Inc., Champaign, IL). Dark calibration of each raw image was performed to remove the dark-current offset from the CCD output. A vessel-tracking algorithm implemented in C++ (Microsoft, Inc., Redmond, WA) and integrated with the software was used to determine the centerline coordinates along the quartz tubes and a series of transverse intensity profiles were obtained orthogonal to the tubes.

For each gray-scale intensity profile, fitting algorithms were used to estimate the intensity at the center of the tube (minima of the nonlinear curve) and the intensity of the background adjacent to the tube (gray-scale value of the linear fit at the center of the tube) to enable an estimate of the optical density of the tube center (Fig. 2), given by

$$OD(\lambda) = -\text{Log}_{10}\left(\frac{I(\lambda)}{I_0(\lambda)}\right) \qquad (1)$$

where, $I(\lambda)$ is the estimated intensity at wavelength λ at the center of the tube, and $I_0(\lambda)$ is the estimate of intensity at the same position

A

Black aluminum outer casing →

Quartz tubes containing human blood →

Chamber of the model eye is filled with distilled water during use →

Front of the model eye with an aperture containing a 62.5D lens →

B

Quartz tube

Lens

Incident light

Spectralon

Water

Aluminum outer casing
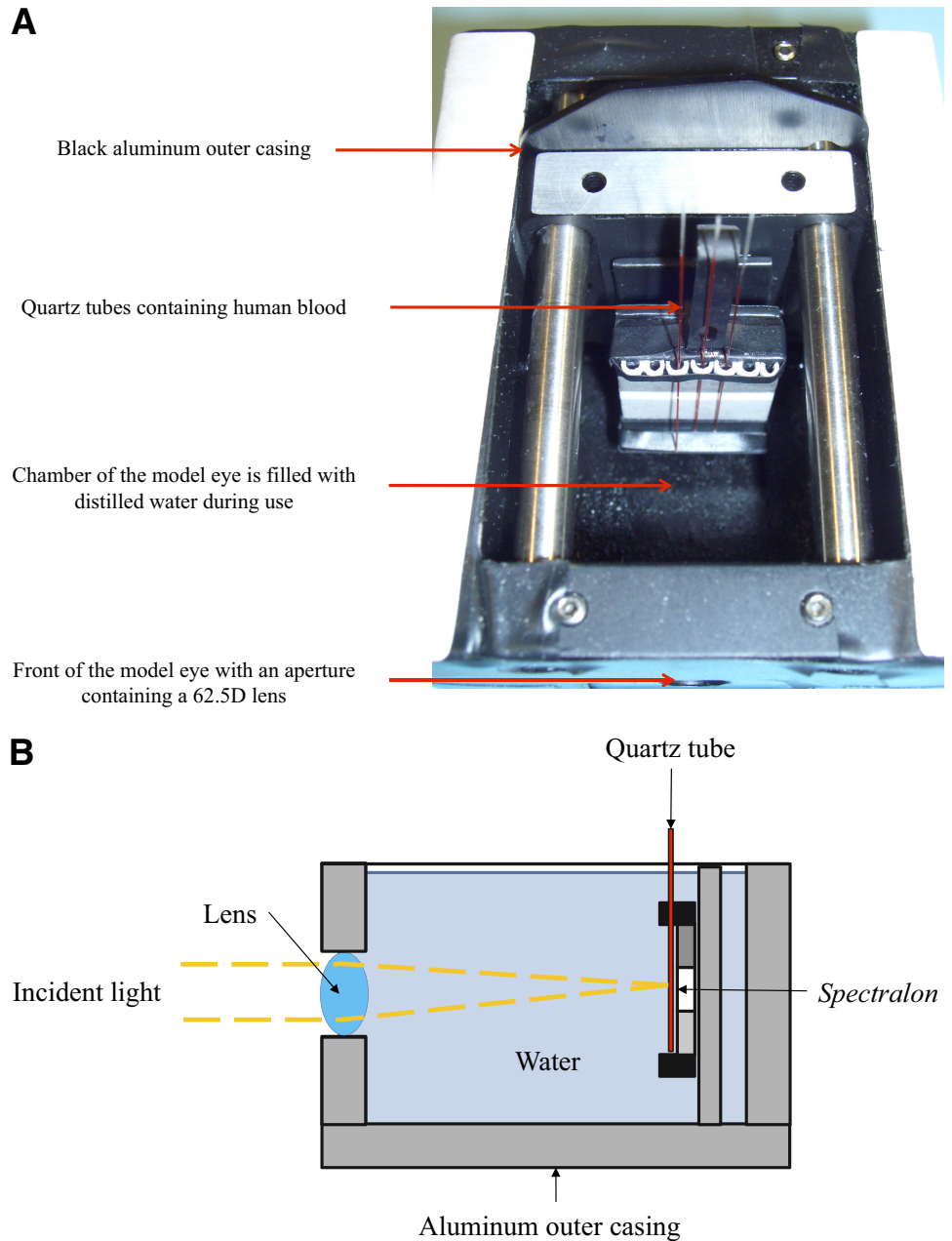
Figure 1. The model eye. (**A**) The model eye viewed from the top containing the reflectance background (Spectralon; Labsphere, North Sutton, NH) and human blood in 150 μm quartz tubes. (**B**) Schematic cross section of the model eye.

obtained by interpolation of the intensities on either side of the tube—that is, an estimate of the intensity in the absence of the tube. The effects of reflections (e.g., specular reflection or refractive index mismatch between the water–quartz–blood interface) on the quartz tubes are minimized by the curve-fitting technique used to estimate the intensity at the center of the blood column. The optical densities of a

Table 1. Number of Blood Sample Types and Quartz Tubes Used in the Model Eye Experiment

Blood Sample Type	Number of Blood-Filled Quartz Tubes Imaged		
	100 μm Tubes	150 μm Tubes	Total
Arterial	2	2	4
Venous	8	8	16
Total	10	10	20

given point were estimated across the wavelength range (500–650 nm) to calculate the optical density spectral variation, $OD(\lambda)$. This process was repeated at multiple points along all the quartz tubes.

Calculation of the oxygen saturation along the length of the quartz tubes was performed by inversion of the complete set of $OD(\lambda)$ given by

$$OD(\lambda) = aS(\lambda) + \eta(\lambda)C_{\text{HbTotal}}d[(\varepsilon_{\text{oxy}}(\lambda) - \varepsilon_{\text{de-oxy}}(\lambda))cOS + \varepsilon_{\text{de-oxy}}(\lambda)]$$

$$(2)$$

where, C_{HbTotal} is the total concentration of hemoglobin, ε_{oxy}, and $\varepsilon_{\text{de-oxy}}$ are the extinction coefficients of oxygenated and deoxygenated hemoglobin[45] respectively corrected for convolution with the spectral response of the liquid crystal tunable filter, d is the vessel diameter, cOS is the calculated oxygen saturation, η is the effective optical path length contribution,[37] and a is a scaling constant. The function S accounts for the backscatter by blood cells. Wavelength-dependent optical scattering values published by Meinke et al.[46] were used in this oximetry model. In

FIGURE 2.   Analysis of the gray-scale intensity profile across a given point in the quartz tube at one wavelength. (**A**) Image from a model experiment taken at 500 nm showing the location of the linear profile across a quartz tube (*red solid line*) to be analyzed. (**B**) A plot of the gray-scale intensities along the linear profile. A curve-fitting algorithm (*blue dashed line*) was applied to the gray-scale intensity profile to estimate the gray-scale intensity at the center of the tube. The value $I(\lambda)$ was determined from the minimum value of the curve. A linear fitting algorithm (*green solid line*) was used to estimate the intensity of the background in the absence of the quartz tube, $I_o(\lambda)$.

essence, this algorithm estimates the free parameters based on the Levenberg-Marquardt nonlinear fit to $OD(\lambda)$, to yield an estimate of cOS.

Statistical Analysis

To determine the effect of the background reflectivity and tube size, we calculated the mean oxygen saturation differences (difference between the measured and calculated oxygen saturation) for segments of the 100 and 150 μm quartz tubes overlying the three different background reflectivities. A repeated-measures, two-way analysis of variance (ANOVA) was performed to compare the effect of tube size and background reflectivity on the mean oxygen saturation difference. A post hoc

power analysis with the mean oxygen saturation difference in each group ($n = 6$; three background reflectivities for each tube size), the average observed SD and a 0.05 significance level was performed with a software program developed by Faul et al.[47] (G*Power, ver. 3.1). Pearson's correlation between the measured oxygen saturation and mean calculated oxygen saturation along the length of each tube were calculated.

The Bland-Altman method[48] was used to assess the agreement between the CO oximeter and the values obtained from equation 2 in 100 μm quartz tubes. The mean calculated oxygen saturation of each segment of the tube overlying the three background reflectivities was calculated, and the mean of the measured and calculated oxygen
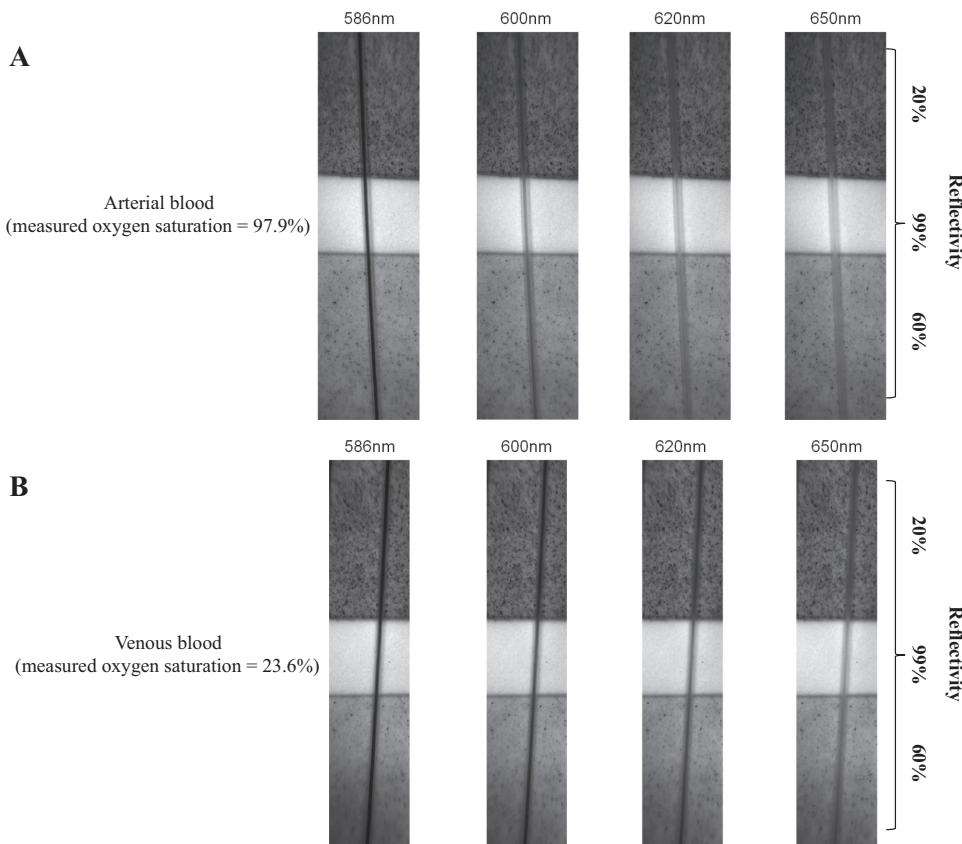
FIGURE 3.   Cropped dark calibrated spectral images of the model eye containing (**A**) arterial and (**B**) venous blood-filled 150 μm quartz tubes. The spectral images shown were acquired at 586, 600, 620 and 650 nm. Each tube is located in front of three reflective grades of the background (Spectralon; Labsphere, North Sutton, NH).

saturation was plotted against the difference between the two methods. Statistical analyses (except the power analysis) were calculated with commercial software (SPSS, ver. 16.0; SPSS Inc., Chicago, IL).

RESULTS

Hyperspectral Images of Arterial and Venous Blood in the Model Eye

Representative narrow-band images of the model eye containing human arterial and venous whole blood in 150 μm quartz tubes obtained at wavelengths of 586, 600, 620 and 650 nm are shown in Figure 3. The vertical dark lines are the quartz tubes containing human blood. Each of the blood-filled quartz tubes spans the three reflective grades of reflectance background. Figure 3A shows a tube containing arterial blood with a measured oxygen saturation of 97.9%. Figure 3B shows a tube containing venous blood with a measured oxygen saturation of 23.6%. It can be observed, as expected, that at the isosbestic wavelength of 586 nm (where the absorbance of oxyhemoglobin and deoxyhemoglobin are equal), both arterial and venous blood appeared to have similar optical densities and that the arterial blood had a lower optical density at wavelengths of 600, 620, and 650 nm than did the venous blood.

Oxygen Saturation Calculation of Blood along the Quartz Tubes

Figures 4 and 5 show the variation of calculated oxygen saturation along the length of 100 μm quartz tubes containing

arterial (measured oxygen saturation = 98%) and venous (measured oxygen saturation = 23%) blood, respectively. Processing and analysis of the model eye images was used to produce a pseudocolor image with a colored representation of the calculated oxygen saturation overlaid on the tube and sequential calculated oxygen saturation values shown to the left of the tube (Figs. 4A, 5A). Examples of the nonlinear fitting of the oximetry model (Figs. 4B, 5B; red lines) to the mean optical density profile along the length of each tube are illustrated with the calculated oxygen saturation. The calculated oxygen saturation values along the length of each tube are also shown in a plot (Figs. 4C, 5C) and demonstrate small fluctuations along its length. These fluctuations were comparatively higher in segments of the arterial and venous blood overlying the 20% reflective background (SD 1.40% and 1.05%, respectively), possibly due to the effect of increased texture in the reflectance background; however, these fluctuations were small. In the quartz tubes containing arterial and venous blood, the mean calculated oxygen saturation along their lengths ($\pm$SD) was 106% $\pm$ 1.13% (n = 1891) and 45% $\pm$ 0.94% (n = 1940), respectively.

Influence of the Background Reflectivity and Quartz Tube Size on the Accuracy of the Calculated Oxygen Saturation

The mean differences between the measured and calculated oxygen saturations for segments of the 100 and 150 μm quartz tubes overlying the different reflective backgrounds are expressed as histograms $\pm$ SEM in Figure 6. A comparison be-
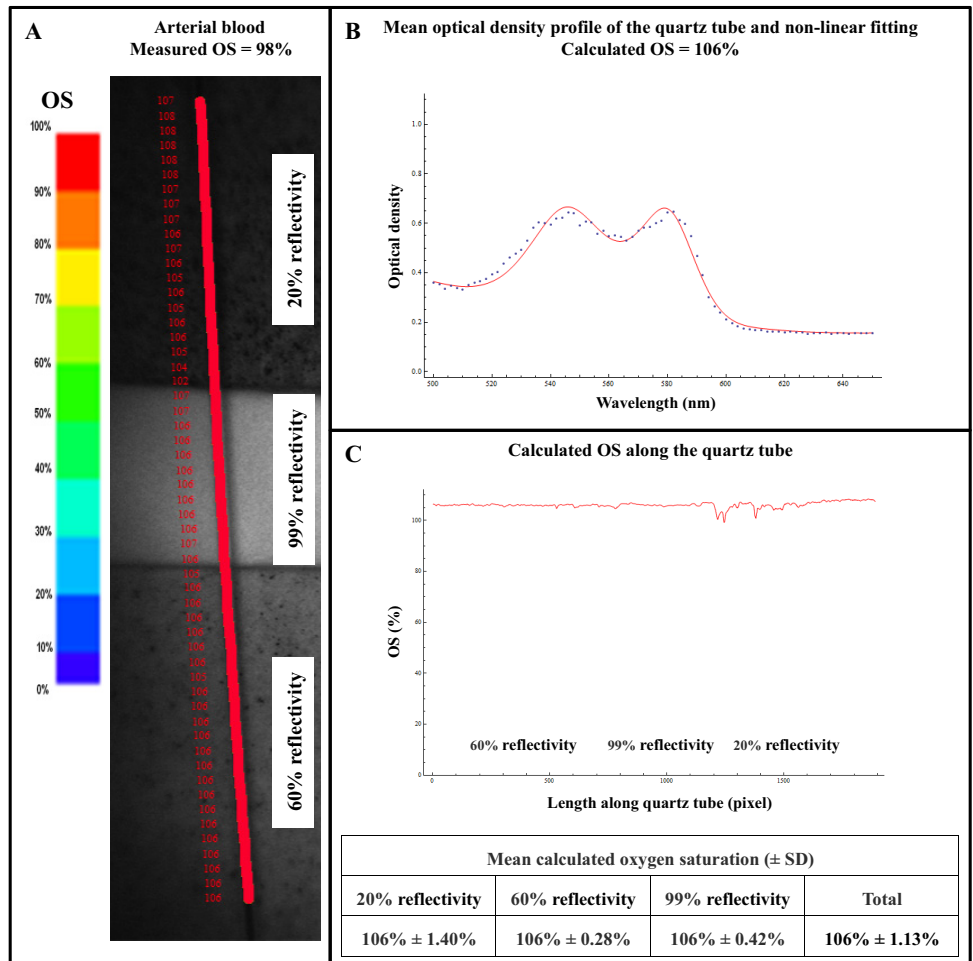
FIGURE 4. Calculated oxygen saturation (OS) along the length of a quartz tube containing arterial blood. (**A**) A cropped pseudocolor image of the model eye with a 100 μm tube containing arterial blood (measured OS = 98%). A colored representation of the calculated OS was overlaid on the tube with sequential levels to the *left* of the tube. (**B**) Mean optical density profile (*blue dots*) of the whole tube and the non–linear-fitting oximetry algorithm (*red line*) to derive the calculated OS (106%). (**C**) Calculated OS (*red line*) along the length of the tube (mean calculated OS $\pm$ SD, 106% $\pm$ 1.13%). The location of the different reflective backgrounds with respect to the calculated OS is indicated in the legends within the graph. The table shows the mean calculated OS ($\pm$SD) of the blood column over segments of the background and along the whole length of the quartz tube.

A Arterial blood Measured OS = 98%

B Mean optical density profile of the quartz tube and non-linear fitting Calculated OS = 106%

C Calculated OS along the quartz tube

Mean calculated oxygen saturation ($\pm$ SD)			
20% reflectivity	**60% reflectivity**	**99% reflectivity**	**Total**
106% $\pm$ 1.40%	**106% $\pm$ 0.28%**	**106% $\pm$ 0.42%**	**106% $\pm$ 1.13%**
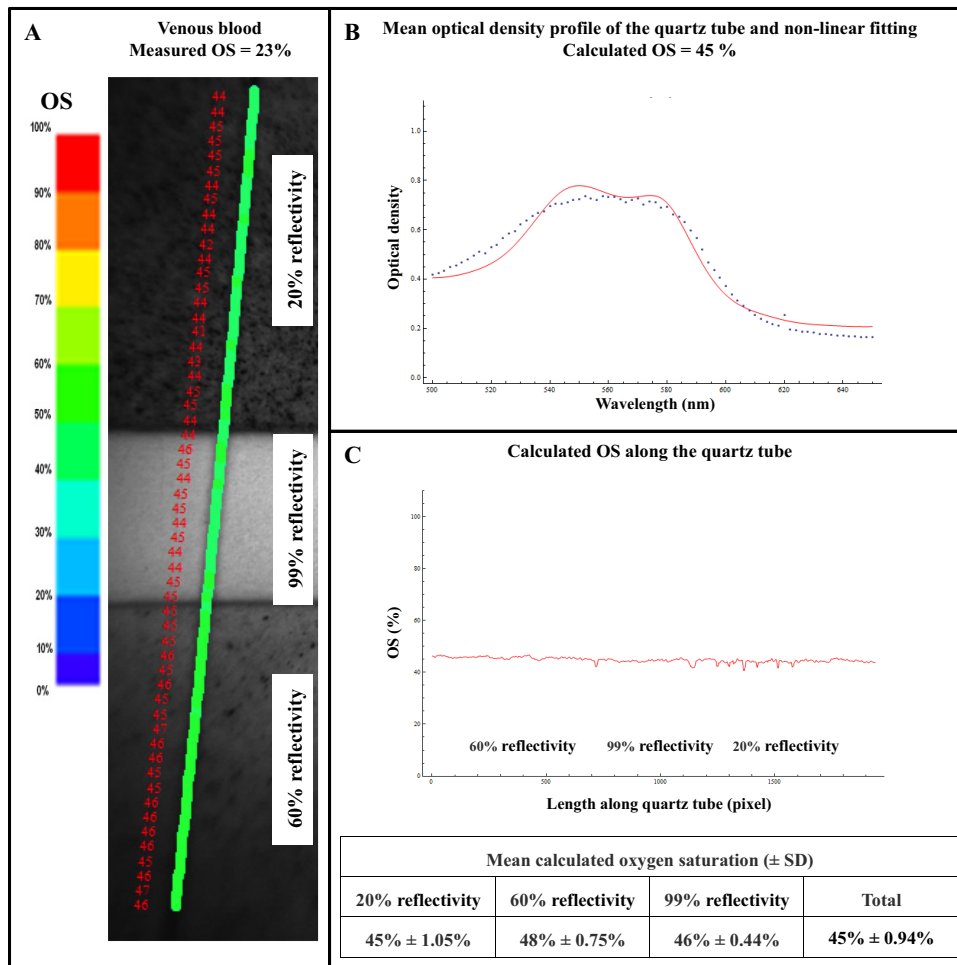
FIGURE 5. Calculated oxygen saturation (OS) along the length of a quartz tube containing venous blood. (A) A cropped pseudocolor image of the model eye with a 100 μm tube containing venous blood (measured OS = 23%). A colored representation of the calculated OS has been overlaid on the tube with sequential values to the *left* of the tube. (B) Mean optical density profile (*blue dots*) of the whole tube and the non-linear fitting oximetry algorithm (*red line*) to derive the calculated OS (45%). (C) Calculated OS (*red line*) along the length of the tube (mean calculated OS $\pm$ SD, 45% $\pm$ 0.94%). The location of the different reflective backgrounds with respect to the calculated OS is indicated in the legends within the graph. The table shows the mean calculated OS ($\pm$SD) of the blood column over segments of the background and along the whole length of the quartz tube.

tween the groups with a two-way ANOVA showed that the degree of reflectance and quartz tube sizes had no significant effects on the mean difference in oxygen saturation ($P = 0.18$ and $P = 0.99$, respectively). The post hoc power calculation of the ANOVA was 0.07.
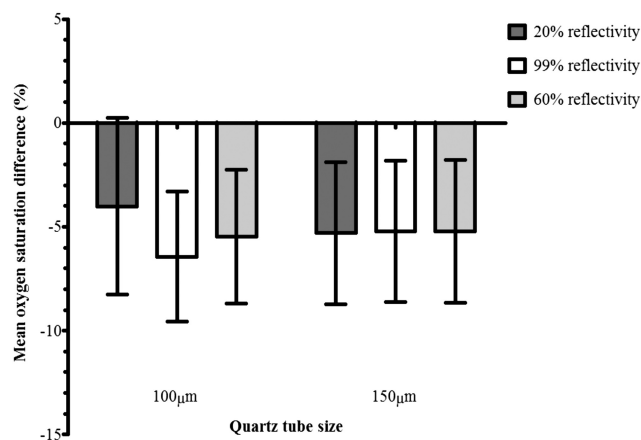
FIGURE 6. Mean differences between the measured and calculated oxygen saturations ($\pm$SEM) in segments of the 100 μm ($n = 10$) and 150 μm ($n = 10$) quartz tubes overlying the three background reflectivities.

Correlation between the Measured and Calculated Oxygen Saturation

A significant and strong correlation between the measured oxygen saturation and respective mean calculated oxygen saturation of all 10 blood-filled 100 μm ($r^2 = 0.96$, $P = 0.000008$) and 10 blood-filled 150 μm ($r^2 = 0.95$, $P = 0.000035$) quartz tubes was found.

Accuracy of the Blood Oxygen Saturation Calculations in the Model Eye

Figure 7 shows Bland-Altman plots for segments of the 100 μm quartz tubes overlying the reflective backgrounds. The mean differences ($\pm$SD) between the measured and calculated oxygen saturations in segments of the 100 and 150 μm tubes overlying the 20%, 60%, and 99% background reflectivities were (100 μm) -4.0% ($\pm13.4\%$), -6.4% ($\pm9.9\%$), and -5.5% ($\pm10.2\%$) and (150 μm) -5.3% ($\pm10.8\%$), -5.2% ($\pm10.7\%$), and -5.2% ($\pm10.9\%$), respectively (95% limits of agreement were -30.2% to 22.3%, -25.9% to 13.0%, and -25.4% to 14.8% for the 100 μm tubes and -26.5% to 15.9%, -26.3% to 15.8%, and -26.5% to 16.1% for the 150 μm tubes).

DISCUSSION

This study demonstrates the ability of our hyperspectral imaging system and oximetry analysis to yield oxygen saturation calculations and evaluates its accuracy with a model eye.
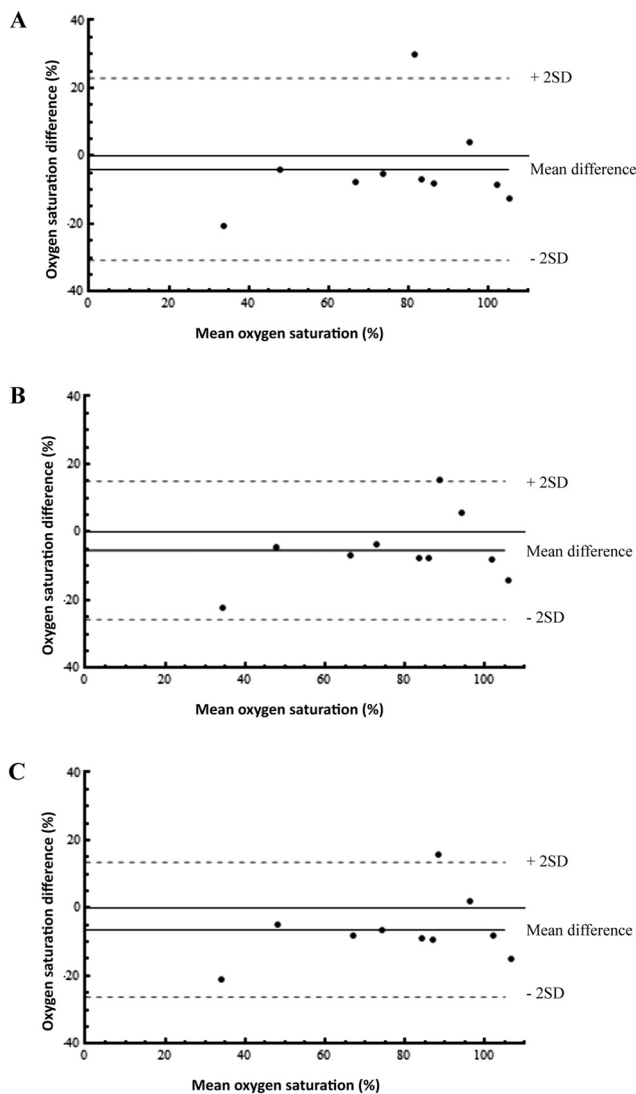
FIGURE 7. Bland-Altman plots showing the agreement between the measured and calculated oxygen saturations in 100 μm quartz tubes. Each plot represents separate analysis of segments of the quartz tubes overlying the three reflective backgrounds: (**A**) 20%, (**B**) 60%, and (**C**) 99%. The mean of each corresponding measured and calculated oxygen saturations are plotted against the difference between the measured and calculated oxygen saturations.

The model eye provided a useful platform to acquire spectral images of blood samples with varying oxygenation. Although it represents a simple optical model of the eye, it has been a useful tool in determining the applicability of hyperspectral imaging to perform oximetry and determine the accuracy of our oximetry model with ground truth, a posteriori knowledge. Figure 3 illustrates an example in which both arterial and venous blood can be visibly distinguished from the dark calibrated spectral images. In this example, both arterial and venous blood appear to have equal optical density at 586 nm; however, at wavelengths of 600, 620 and 650 nm, the arterial blood appears to be optically, less dense than venous blood, probably due to lower extinction coefficients of oxygenated blood at these wavelengths. This finding correlates with published descriptions of the extinction properties of fully oxygenated and fully deoxygenated hemolyzed blood[45]; however, these observations provide only qualitative information regarding the oxygen saturation of blood.

Our quantitative determination of the blood oxygen saturation used a non-linear fitting oximetry model applied to the estimated $OD(\lambda)$ along a given column of blood. We have made attempts to account for variables that influence the propagation of light in the retina, such as scattering by the red blood cells, the optical path length, hemoglobin concentration, and vessel diameter. We have shown that the optical density profiles of arterial and venous blood (Figs. 4B, 5B) are spectrally distinguishable and conform to the published extinction coefficients of fully oxygenated and fully deoxygenated hemoglobin.[45] Furthermore, we have demonstrated that the oximetry model is capable of producing consistent calculated oxygen saturation values along the length of each quartz tube (Figs. 4C, 5C). The SD of the calculated oxygen saturation along each of the quartz tubes shown are small, and the fluctuations in the calculated oxygen saturation values can be explained by the texture in the background reflectance and/or physiological noise (scattering within the blood column due to red blood cells or another component of blood, such as bilirubin, or physiological fluctuations in the oxygen saturation along the blood column). Fluctuations in the calculated oxygen saturation were more prominent in segments of the quartz tubes overlying the 20% reflective background. This effect can be explained by the increased contrast of the texture in the low-albedo reflectance surface (Spectralon; Labsphere, Inc.). Further analysis of the effect of the background reflectivity and tube size on the mean oxygen saturation differences in all quartz tubes was subsequently performed with a repeated-measures, two-way ANOVA. The results indicated that the effect of the background reflectivity and tube size on the mean oxygen saturation differences was not significant ($P = 0.18$ and $P = 0.99$, respectively). The consistency in the calculated oxygen saturation along the length of the quartz tubes (Figs. 4C, 5C) further illustrates the robustness of the oximetry model to variations in the background reflectivities. The oximetry model can therefore be considered to be robust to differences in the background reflectivity and tube diameter. These two features are commonly encountered in the retina, where there are variable vessel diameters and variable amounts of fundus pigmentation resulting in different background reflectivities. The configuration of the reflectance background within the model eye was specifically intended to broadly mimic the variability in fundal pigmentation (20% and 60% background reflectivity from Spectralon) and the optic disc (99% background reflectivity) which is relevant to evaluating the applicability of the oximetry model to a wide population of subjects. The power of the ANOVA was 0.07, according to the post hoc power calculation, and an undetected real difference in the accuracy of the oxygen saturation calculation due to the small sample size could also explain the nonsignificant effect of the background reflectivity and tube size. In addition, the reflectivity of the background cannot be considered to be a precise simulant of the fundus, which has distinct spectral characteristics due to the presence of visual pigments, blood, and other retinal chromophores. Further investigation is needed to determine the accuracy of the oximetry technique in the human eye. A further limitation of this study is that tests of repeatability could not be performed with a high degree of precision. The main reasons for this were, first, that the oxygenation of a given blood sample changed (albeit by a small percentage) over the period between reimaging. Second, the process of imaging the blood samples was performed within a few minutes. From experience, we found that prolonging the imaging process led to segmentation of the blood column in the quartz tubes which could lead to undesirable and uncontrolled changes in the oxygen saturation of the blood column within the tube.

We demonstrated a significant, strong correlation between the measured and calculated oxygen saturation in 100 and 150 μm quartz tubes ($P < 0.01$ in both tube sizes). However, to assess the agreement between the measured and calculated oxygen saturation, we used the Bland-Altman method for each segment of the 100 μm (Fig. 7) and 150 μm quartz tubes overlying the different reflective backgrounds.

The limits of agreement are high from a clinical point of view. It is unlikely that they were affected by the variability of the measured oxygen saturation as the mean difference $\pm$ SD between the measured oxygen saturation, before and after imaging, was small ($0.49\% \pm 0.76\%$). This figure may have been adversely affected by systematic effects. Two plausible ones are: the oxygenation of the blood in the tube may have changed on transfer from the blood gas syringe to the quartz tube; however, this is unlikely, as the transfer of the blood samples to the quartz tubes occurred in a few seconds, and second, and most plausibly, the oximetry model may have overestimated the true oxygen saturation through an imperfect match between the optical model for $OD(\lambda)$ and the data. This is illustrated in Figure 5B, which shows the analysis of a sample of venous blood with a measured oxygen saturation of 23%. The spectral variation in optical density for the whole tube (blue dots) appears to have a distinct bell shape; however, the oximetry model fits a curve to the data that exhibits a distinctive double hump (red line), which is redolent of fully oxygenated blood. It is therefore likely that a fitting error for venous blood contributed to an overestimation of its true oxygen saturation. However, this possible error does not necessarily provide a full explanation of the wide limits of agreement, as it can be observed in Figure 7 that there are two underestimates of the measured oxygen saturation at the higher end of the oxygen saturation scale. It is unlikely that the limits of agreement were affected by the variability of the measured oxygen saturation as the mean difference $\pm$ SD between the measured oxygen saturation before and after imaging was small. In addition, the systematic effect of a fitting error does not address the variability and high SD in the mean differences between the measured and calculated oxygen saturations. Further experiments and evaluation of the fitting technique would be necessary, to establish a comprehensive explanation for our findings. Our future research will initially focus on refining the physical model to remove the effects of this systematic error, particularly at lower oxygen saturations.

The phenomenon of overestimating the true oxygen saturation has been reported in studies on other types of photometric oximeters. Sarnquist et al.[49] reported that pulse oximeters overestimate the actual oxygen saturation, with an average reading of 70% at 50% actual oxygen saturation. This overestimation by pulse oximeters is thought to be caused by the scattering of red or infrared light in the blood vessels.[50] In addition, Drewes et al.[44] reported an error of $\pm52\%$ at 0% blood oxygen saturation in a model eye with an eye oximeter and Delori[22] reported overestimations of the true oxygen saturation, particularly at lower oxygen saturation, in in vitro tests of the retinal vessel oximeter. In light of these results, the accuracy of our oximetry model is comparable to that of those reports. Errors of this magnitude are higher than is desirable, since accuracy in the determination of both the arteriolar and venular oxygen saturation is important in determining the functional status of the inner retina.

This limitation of our oximetry model of lowering blood oxygen saturation could be improved by more accurate characterization of scattering effects within and around the blood column. As a consequence, we have developed and are testing a second-generation model eye that is able to simulate backgrounds of increasing complexities, is able to accommodate tubes manufactured from material with a refractive index close to water, and has a moving blood column allowing smaller tubes to be successfully filled with whole blood. The rationale is to incrementally progress toward a more accurate model of the true optical properties of the human eye until a sufficiently accurate oximetry model can be obtained. Refinement involves a study of light transmission and scattering in and around blood vessels, the retina, and the choroid, with experimental recording and Monte Carlo modeling to inform the construction of a model for the spectral variation in optical densities that can be reliably inverted to yield accurate vessel oximetry.

In conclusion, the model eye has been a useful test bed for evaluating a hyperspectral method of measuring the oxygen saturation of blood with a hyperspectral fundus camera. An accurate oximetry model can be used to determine the oxygen saturation of the retinal vasculature, which has the potential to offer useful functional information on the health of the retina. This model could be implemented to detect, monitor, and assess the outcome of treatments in posterior segment diseases such as glaucoma, diabetic retinopathy, retinovascular occlusions, and age-related macular degeneration.

References

1. Arden GB, Sidman RL, Arap W, Schlingemann RO. Spare the rod and spoil the eye. *Br J Ophthalmol.* 2005;89(6):764–769.
2. Klein R, Klein BEK, Moss SE. The Wisconsin epidemiological study of diabetic retinopathy: a review. *Diabetes Metab Rev.* 1989;5:559–570.
3. Klein BEK, Klein R, Sponsel WE, et al. Prevalence of glaucoma. The Beaver Dam Eye Study. *Ophthalmology.* 1999;99:1499–1504.
4. Quigley H. The number of persons with glaucoma worldwide. *Br J Ophthalmol.* 1996;80:389–393.
5. Vinding T. Visual impairment of age-related macular degeneration: an epidemiological study of 1000 aged individuals. *Acta Ophthalmol.* 1990;68:162–167.
6. Rosenberg T, Klie F. The incidence of registered blindness caused by age-related macular degeneration. *Acta Ophthalmol Scand.* 1996;74:399–402.
7. Ciulla TA, Harris A, Latkany P, et al. Ocular perfusion abnormalities in diabetes. *Acta Ophthalmol Scand.* 2002;80:468–477.
8. Arend O, Wolf S, Jung F, et al. Retinal microcirculation in patients with diabetes mellitus: dynamic and morphological analysis of perifoveal capillary network. *Br J Ophthalmol.* 1991;75(9):514–518.
9. Cioffi GA, Wang L, Fortune B, et al. Chronic ischemia induces regional axonal damage in experimental primate optic neuropathy. *Arch Ophthalmol.* 2004;122(10):1517–1525.
10. Flammer J, Orgül S, Costa VP, et al. The impact of ocular blood flow in glaucoma. *Prog Retin Eye Res.* 2002;21(4):359–393.
11. Friedman E, Krupsky S, Lane A, et al. Ocular blood flow velocity in age-related macular degeneration. *Ophthalmology.* 1995;102:640–646.
12. Chen J, Fitzke F, Pauleikhoff D, Bird A. Functional loss in age-related Bruch's membrane change with choroidal perfusion defect. *Invest Ophthalmol Vis Sci.* 1992;33:334–340.
13. Stefansson E, Machemer R, de Juan E, McCuen BW II. Retinal oxygenation and laser treatment in patients with diabetic retinopathy. *Am J Ophthalmol.* 1992;113:36–38.
14. Lo, L.-W., Koch CJ, Wilson DF. Calibration of oxygen-dependent quenching of the phosphorescence of Pd-meso-tetra [4-carboxylphenyl] porphine: a phosphor with general application for measuring oxygen concentration in biological systems. *Anal Biochem.* 1996;236:153–160.

15. Shonat RD, Wilson DF, Riva CE, Pawlowski M. Oxygen distribution in the retinal and choroidal vessels of the cat as measured by a new phosphorescence imaging method. *Appl Opt.* 1992;31:3711–3718.

16. Zuckerman R. Optical mapping of inner retinal tissue P02. *Curr Eye Res.* 1993;12:809–825.

17. Duong TQ, Ngan SC, Ugurbil K, Kim SG. Functional magnetic resonance imaging of the retina. *Invest Ophthalmol Vis Sci.* 2002;43(4):1176–1181.

18. Hickam JB, Frayser R, Ross JC. A study of retinal venous blood oxygen saturation in human subjects by photographic means. *Circulation.* 1963;27:375–385.

19. Hickam JB, Sicker HO, Frayser R. Studies of retinal circulation and A-V oxygen difference in man. *Trans Am Clin Climatol Assoc.* 1959;71:34–44.

20. Tiedeman JS, Kirk SE, Srinivas S, Beach JM. Retinal oxygen consumption during hyperglycemia in patients with diabetes without retinopathy. *Ophthalmology.* 1998;105:31–36.

21. Beach JM, Schwenzer KJ, Srinivas S, Kirn D, Tiedeman JS. Oximetry of retinal vessels by dual-wavelength imaging: calibration and influence of pigmentation. *J Appl Physiol.* 1999;86:748–758.

22. Delori FC. Noninvasive technique for oximetry of blood in retinal vessels. *Appl Opt.* 1988;27(6):1113–1125.

23. Hardarson SH, Harris A, Karlsson RA, et al. Automatic retinal oximetry. *Invest Ophthalmol Vis Sci.* 2006;47(11):5011–5016.

24. Crittin M, Schmidt H, Riva CE. Hemoglobin oxygen saturation (SO2) in the human ocular fundus measured by reflectance oximetry: preliminary data in retinal veins. *Klin Monatsbl Augenheilkd.* 2002;219:289–291.

25. Nelson DA, Krupsky S, Pollack A, et al. Special report: noninvasive multi-parameter functional optical imaging of the eye. *Ophthalmic Surg Lasers Imaging.* 2005;36(1):57–66.

26. Ramella-Roman JC, Mathews SA, Kandimalla H, et al. Measurement of oxygen saturation in the retina with a spectroscopic sensitive multi aperture camera. *Opt Express.* 2008;28:16(9):6170–6182.

27. Hirohara Y, OKawa Y, Mihashi T, et al. Validity of retinal oxygen saturation analysis: hyperspectral imaging in visible wavelength with fundus camera and liquid crystal wavelength tunable filter. *Opt Rev.* 2007;14(3):151–158.

28. Schweitzer D, Leistritz L, Hammer M, Scibor M, Bartsch U, Strobel J. Calibration-free measurement of the oxygen saturation in retinal vessels of men: ophthalmic technologies V. *Proc SPIE.* 1995;2393:210–218.

29. Schweitzer D, Hammer M, Kraft J, Thamm E, Konigsdorffer E, Strobel J. In vivo measurement of the oxygen saturation of retinal vessels in healthy volunteers. *IEEE Tram Biomed Eng.* 1999;46:1454–1465.

30. Schweitzer D, Thamm E, Hammer M, Kraft J. A new method for the measurement of oxygen saturation at the human ocular fundus. *Int Ophthalmol.* 2001;23:347–353.

31. Michelson G, Scibor M. Intravascular oxygen saturation in retinal vessels in normal subjects and open-angle glaucoma subjects. *Acta Ophthalmol Scand.* 2006;84:89–295.

32. Khoobehi B, Beach JM, Kawano H. Hyperspectral imaging for measurement of oxygen saturation in the optic nerve head. *Invest Ophthalmol Vis Sci.* 2004;45(5):1464–1472.

33. Yoneya S, Saito T, Nishiyama Y, et al. Retinal oxygen saturation levels in patients with central retinal vein occlusion. *Ophthalmology.* 2002;109(8):1521–1526.

34. Johnson WR, Wilson DW, Fink W, Humayun M, Bearman G. Snapshot hyperspectral imaging in ophthalmology. *J Biomed Opt.* 2007;12(1):014036.

35. Smith MH, Denninghoff KR, Lompado A, Woodruff JB, Hillman LW. Minimizing the influence of fundus pigmentation on retinal vessel oximetry measurements: ophthalmic technologies XI. *Proc SPIE.* 2001;4245:135–145.

36. Smith MH, Denninghoff KR, Lompado A, Hillman LW. Retinal vessel oximetry: toward absolute calibration: ophthalmic technologies X. *Proc SPIE.* 2000;3908:217–226.

37. Smith MH, Denninghoff KR, Lompado A, Hillman LW. Effect of multiple light paths on retinal vessel oximetry. *Appl Opt.* 2000;29:1183–1193.

38. Denninghoff KR, Smith MH, Hillman L. Retinal imaging techniques in diabetes. *Diabetes Technol Ther.* 2000;2:111–113.

39. Heaton LC, Smith MH, Denninghoff KR, Hillman LW. Handheld four-wavelength retinal vessel oximeter: ophthalmic technologies X. *Proc SPIE.* 2000;3908:227–233.

40. Ashman RA, Reinholz F, Eikelboom RH. Oximetry with a multiple wavelength SLO. *Int Ophthalmol.* 2001;23(4–6):343–346.

41. Kagemann L, Wollstein G, Wojtkowski M, et al. Spectral oximetry assessed with high-speed ultra-high-resolution optical coherence tomography. *J Biomed Opt.* 2007;12(4):041212.

42. Hickam JB, Frayser R. Spectrophotometric determination of blood oxygen. *J Biol Chem.* 1949;180(1):457–465.

43. de Kock JP, Tarassenko L, Glynn CJ, Hill AR. Reflectance pulse oximetry measurements from the retinal fundus. *IEEE Trans Biomed Eng.* 1993;40(8):817–823.

44. Drewes J, Smith MH, Denninghoff KR, Hillman LW. An instrument for the measurement of retinal vessel oxygen saturation: optical diagnostics of biological fluids IV. *Proc SPIE.* 1999;3591:114–120.

45. van Assendelft OW. *Spectroscopy of Hemoglobin Derivatives.* Springfield, IL: C. C. Thomas; 1970.

46. Meinke M, Müller G, Helfmann J, Friebel M. Empirical model functions to calculate hematocrit-dependent optical properties of human blood. *Appl Opt.* 2007;46(10):1742–1753.

47. Faul F, Erdfelder E, Buchner A, Lang AG. Statistical power analyses using G*Power 3.1: tests for correlation and regression analyses. *Behav Res Methods.* 2009;41:1149–1160.

48. Bland JM, Altman DG. Statistical methods for assessing agreement between 2 methods of clinical measurement. *Lancet.* 1986;1:307–310.

49. Sarnquist F, Todd C, Whitcher C. Accuracy of a new non-invasive oxygen saturation monitor. *Anesthesiology.* 1980;53:S163.

50. Shimada Y, Yoshiya I, Oka N, Hamaguri K. Effects of multiple scattering and peripheral circulation on arterial oxygen saturation measured with a pulse-type oximeter. *Med Biol Eng Comput.* 1984;22:475–478.